

Dynamic modeling and simulation of a parallel planar mechanism using bond graph (power flow) approach

Albuquerque, A. N.¹, Speranza Neto, M.¹, Meggiolaro, M. A.¹

¹ Pontifical Catholic University, Department of Mechanical Engineering, Rua Marquês de São Vicente, 225, CEP 22241-900, Gávea, Rio de Janeiro, RJ, Brazil, allan@puc-rio.br, msn@puc-rio.br, meggi@puc-rio.br

Abstract: This work presents the analytical form determination of the dynamic model of a parallel planar mechanism with three degrees of freedom through the characterization of the power flow between its components. From the geometrical relations associated to the displacement of their degrees of freedom, the kinematic relations associated to their speeds are determined. Considering the power flow between the degrees of freedom, and also between these and the actuating elements (linear electric actuators) the equilibrium relations of the forces and torques are obtained. Accounting for inertial effects of system components, the stiffness and damping effects, the equations of motion or the state equations are analytically determined. Besides, the relation between the inverse kinematics and the direct dynamics is presented. The proposed methodology is generalized and applicable in any type of mechanism (open or closed, planar or spatial). In this work, the vector loop technique is used to determine the inverse geometric model, and with its derivation, the kinematic relations are obtained, and therefore the inverse Jacobian matrix. Thereby, the inverse kinematics bond graph is built and, from the cause and effect relations, the direct dynamic model of the mechanism is found. Thus, this methodology (bond graphs or power flow) is more efficient and secure to achieve the dynamic analytical (closed) models of parallel mechanisms. A set of simulations are performed to validate this approach, using the real data (geometry, inertia, damping, actuators forces, etc.) from a planar mechanism designed and built especially for the purpose to compare the simulated and experimental results. The analytical equations lead to a more efficient simulation process and real-time control of these systems.

Keywords: Parallel Mechanisms, Inverse Kinematic, Direct Dynamic, Power Flow, Causal Relations, Bond Graphs

INTRODUCTION

Mechanisms are essentially (but not exclusively) made up of multiple rigid bodies that have relative motion between themselves. Each rigid body is connected through a joint to one or more bodies, wherein the serial sequence of connected bodies is called kinematic chain. Open kinematic chains have no restrictions on their ends, as closed chains have restrictions on both ends. In this work, the focus will be given on the study of mechanisms with closed kinematic chains. Despite of having a smaller workspace, higher inertia and a harder dynamic analysis, parallel systems have great advantages when compared to serial manipulators, as better stability and accuracy, ability to handle relatively large loads, high velocities and accelerations and low power operation (Wang, 2008).

The proposed methodology is generalized and applicable in any type of mechanism (open or closed, planar or spatial). For a better comprehension of the methodology, a planar case will be discussed in this work. The inverse kinematic model of the closed chain mechanism, which has easy solution when compared to the direct model, can be developed by any known methodology, without the need for a systematic approach. It begins by determining the inverse geometric model and its derivation to obtain the kinematic relations, and therefore the inverse Jacobian matrix. With the inverse kinematic model, the inverse kinematics bond graph is built and, from the cause and effect relations, the direct dynamic model of the mechanism is found. Thus, this methodology (bond graphs or power flow) is more efficient and secure to achieve the dynamic analytical (closed) models of parallel mechanisms. For the purpose of provide real data (geometry, inertia, damping, actuators forces, etc.) and compare the simulated and experimental results, a planar mechanism was designed and built. Figure 1.a shows the CAD model of the planar mechanism and Fig. 1.b shows the built platform.



Figure 1 – CAD model of the planar mechanism (a) and the built platform (b).

This procedure is based on the Bond Graph Technique and all its potential for the development of modules' models. However the formalism and the graphical representation of Bond Graphs are no longer needed once the model of one module is built, as a function of the power flow and of the causality relations among their internal elements and mainly as a function of the elements in the power input and power output ports. Thus the module can be coupled to other modules whose models were created observing such restrictions and therefore the analytical model of a system constructed from multiple subsystems may be easily established by the consistent combination in terms of power and causality, avoiding the necessity of apply the formal treatment of the Bond Graph Technique (Martins *et al.*, 2016).

INVERSE KINEMATICS OF THE PLANAR PLATFORM

Figure 2 shows the 3-RPR parallel manipulator considered in this study. Three limbs connects to the mobile platform and the fixed base by rotational joints in points B_i and A_i , $i = 1, 2 e 3$. To describe its geometry, a referential frame $A(X, Y)$ fixed to the platform base is added and other frame, $B(x, y)$, is coupled to the mobile platform. Another reference frame, $C(x_i, y_i)$, is fixed to each rotational joint, thus having its origin at the point A_i ($i = 1, 2 e 3$). The y_i axis of this system points from A_i to B_i (direction of the actuator i). For convenience, the origin of the frame B is located at the center of the mobile platform. The position of the mobile platform can be described by the vector $\mathbf{p} = [p_x, p_y]^T = [X, Y]^T$ and by the rotation matrix ${}^A\mathbf{R}_B$. Hence, the velocities state of the mobile platform is defined as a three dimensional vector with the absolute linear velocity and the angular velocity of the mobile platform (Eq. 1).

$$\dot{\mathbf{x}} = \mathbf{v} = \begin{bmatrix} \mathbf{v}_p \\ \boldsymbol{\omega}_p \end{bmatrix} = \begin{bmatrix} \dot{X} \\ \dot{Y} \\ \dot{\theta} \end{bmatrix} = \begin{bmatrix} v_x \\ v_y \\ \omega_z \end{bmatrix} \tag{1}$$

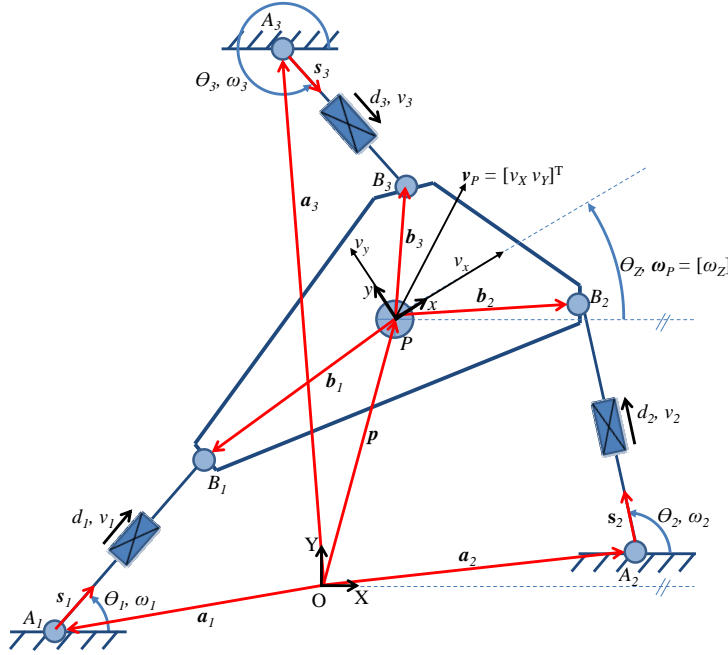


Figure 2 – Planar platform with three degrees of freedom.

For this manipulator, the input vector is given by $\mathbf{v}_A = [v_1, v_2, v_3]^T$ and the output vector can be described by the centroid velocity P and the angular velocity of the mobile platform, $\mathbf{v} = [v_x, v_y, \omega_z]^T$. Using the vector loop technique and then, applying the differential with respect to time, the relationship between the variables which describe the angular and linear velocity of the mobile platform and the velocities of the links of the planar platform is found. With this relation, the inverse Jacobian of the manipulator is obtained, as shown in Eq. 2 (Albuquerque *et al.*, 2016).

$$\dot{\mathbf{q}} = \begin{bmatrix} \dot{d}_1 \\ \dot{d}_2 \\ \dot{d}_3 \end{bmatrix} = \begin{bmatrix} v_1 \\ v_2 \\ v_3 \end{bmatrix} = \mathbf{J}^{-1} \dot{\mathbf{x}} = \begin{bmatrix} \cos \theta_1 & \sin \theta_1 & b_{1X} \sin \theta_1 - b_{1Y} \cos \theta_1 \\ \cos \theta_2 & \sin \theta_2 & b_{2X} \sin \theta_2 - b_{2Y} \cos \theta_2 \\ \cos \theta_3 & \sin \theta_3 & b_{3X} \sin \theta_3 - b_{3Y} \cos \theta_3 \end{bmatrix} \begin{bmatrix} \dot{X} \\ \dot{Y} \\ \dot{\theta} \end{bmatrix} \tag{2}$$

in which θ_i are given by Eq. 3 (with $i = 1, 2$ and 3).

$$\theta_i = \tan^{-1} \left(\frac{b_{iY} - a_{iY}}{b_{iX} - a_{iX}} \right) = \tan^{-1} \left(\frac{Y + b_{iX} \sin \theta + b_{iY} \cos \theta - a_{iY}}{X + b_{iX} \cos \theta - b_{iY} \sin \theta - a_{iX}} \right) \tag{3}$$

Rewriting Eq. 2 in function of $\tan(\theta_i)$, differentiating both sides, and manipulating the terms in order to put in evidence the absolute linear velocities and angular velocity of the platform, we obtain the inverse Jacobian that relates these velocities to the angular velocity of each of the members (Albuquerque *et al.*, 2016). Equation 4 presents that relation the terms of the matrix.

$$\dot{\theta} = \begin{bmatrix} \dot{\theta}_1 \\ \dot{\theta}_2 \\ \dot{\theta}_3 \end{bmatrix} = \omega_A = \begin{bmatrix} \omega_1 \\ \omega_2 \\ \omega_3 \end{bmatrix} = \mathbf{J}_\theta^{-1} \begin{bmatrix} v_X \\ v_Y \\ \omega_Z \end{bmatrix} = \begin{bmatrix} \frac{(a_{1Y}-b_{1Y})\cos^2(\theta_1)}{(b_{1X}-a_{1X})^2} & \frac{\cos^2(\theta_1)}{(b_{1X}-a_{1X})} & \frac{\cos^2(\theta_1)}{(b_{1X}-a_{1X})^2} j_{\theta 1} \\ \frac{(a_{2Y}-b_{2Y})\cos^2(\theta_2)}{(b_{2X}-a_{2X})^2} & \frac{\cos^2(\theta_2)}{(b_{2X}-a_{2X})} & \frac{\cos^2(\theta_2)}{(b_{2X}-a_{2X})^2} j_{\theta 2} \\ \frac{(a_{3Y}-b_{3Y})\cos^2(\theta_3)}{(b_{3X}-a_{3X})^2} & \frac{\cos^2(\theta_3)}{(b_{3X}-a_{3X})} & \frac{\cos^2(\theta_3)}{(b_{3X}-a_{3X})^2} j_{\theta 3} \end{bmatrix} \begin{bmatrix} \dot{X} \\ \dot{Y} \\ \dot{\theta} \end{bmatrix} \quad (4)$$

$j_{\theta i}$ are given by Eq. 5, with $i = 1, 2, 3$, $c\theta = \cos(\theta)$ and $s\theta = \sin(\theta)$.

$$j_{\theta i} = (b_{ix} c \theta - b_{iy} s \theta)(b_{iX}-a_{iX}) + (b_{ix} s \theta + b_{iy} c \theta)(b_{iY}-a_{iY}) \quad (5)$$

In order to obtain the relation between the linear and angular velocities and accelerations of the moving platform and the linear accelerations of the actuators of the mechanism, the differential of the inverse Jacobian has to be calculated, as shown in Eq. 6. The matrix of the derivatives of the inverse Jacobian is given by Eq. 7.

$$\ddot{q} = \begin{bmatrix} \dot{v}_1 \\ \dot{v}_2 \\ \dot{v}_3 \end{bmatrix} = \begin{bmatrix} a_1 \\ a_2 \\ a_3 \end{bmatrix} = \dot{\mathbf{J}}^{-1} \dot{x} + \mathbf{J}^{-1} \ddot{x} = \dot{\mathbf{J}}^{-1} \begin{bmatrix} v_X \\ v_Y \\ \omega_Z \end{bmatrix} + \mathbf{J}^{-1} \begin{bmatrix} a_X \\ a_Y \\ a_Z \end{bmatrix} \quad (6)$$

$$\dot{\mathbf{J}}^{-1} = \begin{bmatrix} -s \theta_1 \dot{\theta}_1 & c \theta_1 \dot{\theta}_1 & b_{1X} s \theta_1 - b_{1Y} c \theta_1 + b_{1X} c \theta_1 \dot{\theta}_1 + b_{1Y} s \theta_1 \dot{\theta}_1 \\ -s \theta_2 \dot{\theta}_2 & c \theta_2 \dot{\theta}_2 & b_{2X} s \theta_2 - b_{2Y} c \theta_2 + b_{2X} c \theta_2 \dot{\theta}_2 + b_{2Y} s \theta_2 \dot{\theta}_2 \\ -s \theta_3 \dot{\theta}_3 & c \theta_3 \dot{\theta}_3 & b_{3X} s \theta_3 - b_{3Y} c \theta_3 + b_{3X} c \theta_3 \dot{\theta}_3 + b_{3Y} s \theta_3 \dot{\theta}_3 \end{bmatrix} \quad (7)$$

b_{iX} and b_{iY} are given by Eq. 8 and 9, respectively, for $i = 1, 2$ and 3.

$$b_{iX} = v_X - \omega_Z (b_{ix} s \theta + b_{iy} c \theta) \quad (8)$$

$$b_{iY} = v_Y + \omega_Z (b_{ix} c \theta - b_{iy} s \theta) \quad (9)$$

The same method is applied with the relation between the velocities and accelerations of the moving platform and the angular accelerations of the actuators (Eq. 10). The matrix of the derivatives of \mathbf{J}_θ^{-1} is given by Eq. 11.

$$\dot{\theta} = \begin{bmatrix} \dot{\omega}_1 \\ \dot{\omega}_2 \\ \dot{\omega}_3 \end{bmatrix} = \begin{bmatrix} \alpha_1 \\ \alpha_2 \\ \alpha_3 \end{bmatrix} = \dot{\mathbf{J}}_\theta^{-1} \dot{x} + \mathbf{J}_\theta^{-1} \ddot{x} = \dot{\mathbf{J}}_\theta^{-1} \begin{bmatrix} v_X \\ v_Y \\ \omega_Z \end{bmatrix} + \mathbf{J}_\theta^{-1} \begin{bmatrix} a_X \\ a_Y \\ a_Z \end{bmatrix} \quad (10)$$

$$\dot{\mathbf{J}}_\theta^{-1} = \begin{bmatrix} \dot{J}_{\theta 11}^{-1} & \dot{J}_{\theta 12}^{-1} & \dot{J}_{\theta 13}^{-1} \\ \dot{J}_{\theta 21}^{-1} & \dot{J}_{\theta 22}^{-1} & \dot{J}_{\theta 23}^{-1} \\ \dot{J}_{\theta 31}^{-1} & \dot{J}_{\theta 32}^{-1} & \dot{J}_{\theta 33}^{-1} \end{bmatrix} \quad (11)$$

$\dot{J}_{\theta 11}^{-1}$, $\dot{J}_{\theta 12}^{-1}$ and $\dot{J}_{\theta 13}^{-1}$ are given by Eq. 12, 13 and 14, respectively, for $i = 1, 2$ and 3.

$$\dot{J}_{\theta 11}^{-1} = \frac{[2c\theta_i s\theta_i \omega_i (b_{iY}-a_{iY}) - b_{iY} c^2 \omega_i] (b_{iX}-a_{iX}) - 2b_{iX} (a_{iY}-b_{iY}) c^2 \theta_i}{(b_{iX}-a_{iX})^3} \quad (12)$$

$$\dot{J}_{\theta 12}^{-1} = \frac{2c\theta_i s\theta_i \omega_i (a_{iX}-b_{iX}) - b_{iX} c^2 \theta_i}{(b_{iX}-a_{iX})^2} \quad (13)$$

$$\dot{J}_{\theta 13}^{-1} = \frac{[j_{\theta i} c^2 \theta_i - 2c\theta_i s\theta_i \omega_i j_{\theta i}] (b_{iX}-a_{iX}) - 2b_{iX} j_{\theta i} c^2 \theta_i}{(b_{iX}-a_{iX})^3} \quad (14)$$

$\dot{j}_{\theta i}$ are given by Eq. 15 for $i = 1, 2$ and 3.

$$\dot{j}_{\theta i} = (b_{iy} c \theta - b_{ix} s \theta)(b_{ix} - a_{ix})\omega_Z + (b_{ix} c \theta + b_{iy} s \theta)\dot{b}_{ix} + (b_{ix} c \theta - b_{iy} s \theta)(b_{iy} - a_{iy})\omega_Z + (b_{ix} s \theta + b_{iy} c \theta)\dot{b}_{iy} \quad (15)$$

As in the bond graph speed restrictions may be imposed directly, one can build the bond graph for the kinematics system analysis before mounting the graph for dynamic analysis. In a graph that correctly describes the kinematics (1 and 0 junctions, transformers and gyrators), the dynamics (capacitors, inertias and resistors) can be imposed without the risk of creating models where the main constraints of mechanical systems are violated: geometric or kinematic ties (Speranza Neto and Silva, 2005).

In this model, speed conditions are imposed by ideal velocity sources, that is, a source of velocity for v_x , v_y and ω_z . Besides these velocities, the others 1 junctions (of common velocities) indicates the linear (v_1 , v_2 e v_3) and angular velocities (ω_1 , ω_2 e ω_3) of the actuators. Thus, the inverse kinematics of the planar platform via bond graphs is represented as shown in Fig. 3, whereby the modulated transformer type two-port elements indicated by \mathbf{J}_{ij}^{-1} and \mathbf{J}_{0ij}^{-1} represents the matrices \mathbf{J}^{-1} (Eq. 2) and \mathbf{J}_0^{-1} (Eq. 4) terms of row i and column j , respectively. Figure 4 shows the same model using multibond graphs.

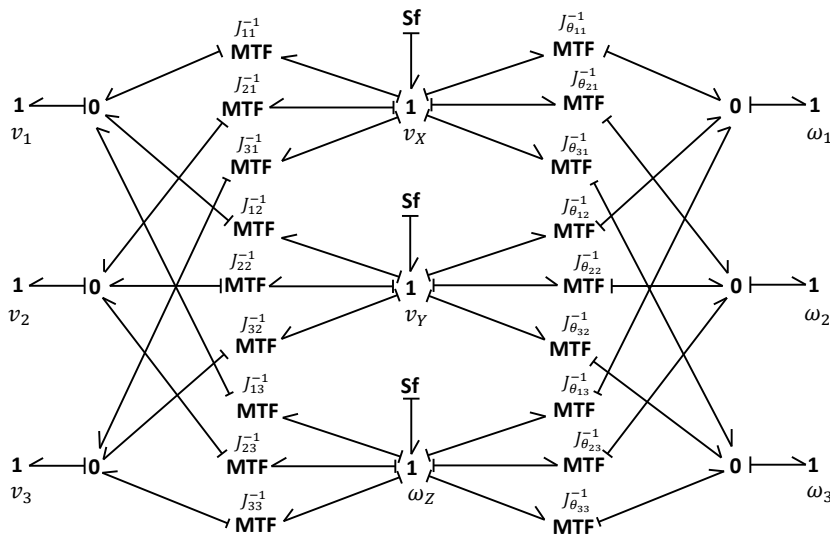


Figure 3 – Bond graphs representation of the planar platform inverse kinematics.

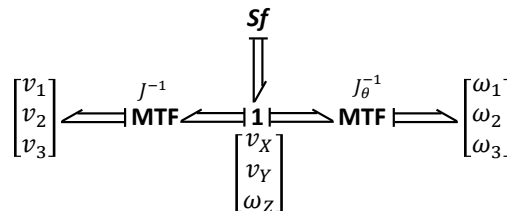


Figure 4 – Multibond graphs representation of the planar platform inverse kinematics.

Inverse kinematic model validation

A set of simulations were made to validate the inverse geometric model (vector loop equation) and the inverse kinematic model (using the matrices \mathbf{J}^{-1} and \mathbf{J}_0^{-1}). Table 1 presents the geometric parameters of the mechanism and Figure 5 shows two different configurations of the planar mechanism in the *MatLab/Simulink* simulation environment: the initial condition, where $[X Y \theta] = [0.0 0.0 0.262]$ (a) and a configuration where $[X Y \theta] = [20.0 30.0 0.262]$ (b), with X and Y in mm and θ in rad.

Table 1 – Geometric parameters.

Identification	Symbol	Value
A ₁ joint coordinates in reference frame A (mm)	a_1	[-389.14 -224.67]
A ₂ joint coordinates in reference frame A (mm)	a_2	[389.14 -224.67]
A ₃ joint coordinates in reference frame A (mm)	a_3	[0.00 449.34]
B ₁ joint coordinates in reference frame B (mm)	b_1	[-125.00 -72.17]
B ₂ joint coordinates in reference frame B (mm)	b_2	[125.00 -72.17]
B ₃ joint coordinates in reference frame B (mm)	b_3	[0.00 144.34]
Linear actuator fixed length (mm)	L_{min}	255.00
Stroke of the linear actuator (mm)	S	100.00

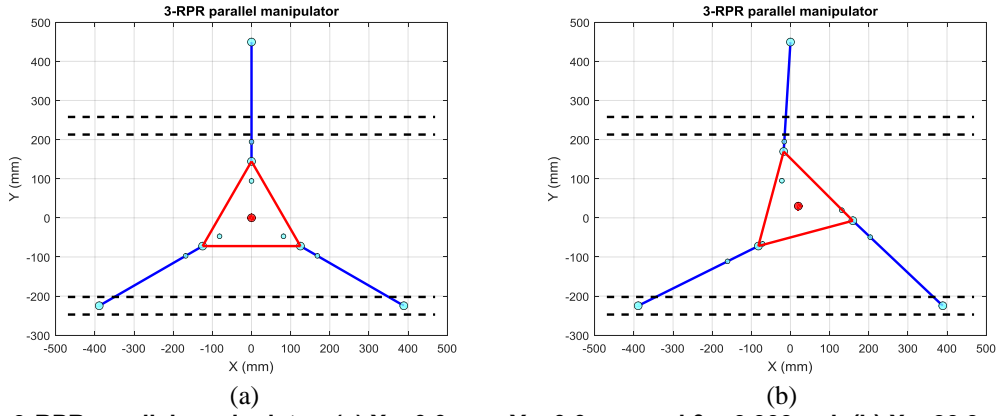


Figure 5 – 3-RPR parallel manipulator: (a) $X = 0.0$ mm, $Y = 0.0$ mm and $\theta = 0.000$ rad; (b) $X = 20.0$ mm, $Y = 30.0$ mm and $\theta = 0.262$ rad (15.0°).

Using the Jacobian matrices from the Eq. 2 and 4, the time response of the limbs was obtained for the input functions shown in Eq. 16. Figures 6.b and 6.d shows the linear and angular velocities of the actuators, respectively, obtained directly from the Jacobian matrices. Figure 6.a and 6.c shows the linear and angular displacements of the actuators, respectively, by integrating (with the corresponding boundary conditions) the velocities of the actuators.

$$\begin{cases} \dot{X} = 50.00\sin(\pi t) \text{ mm/s} \\ \dot{Y} = 50.00\sin(\pi t) \text{ mm/s} \\ \dot{\theta} = 0.785\sin(\pi t) \text{ rad/s} \end{cases} \quad (16)$$

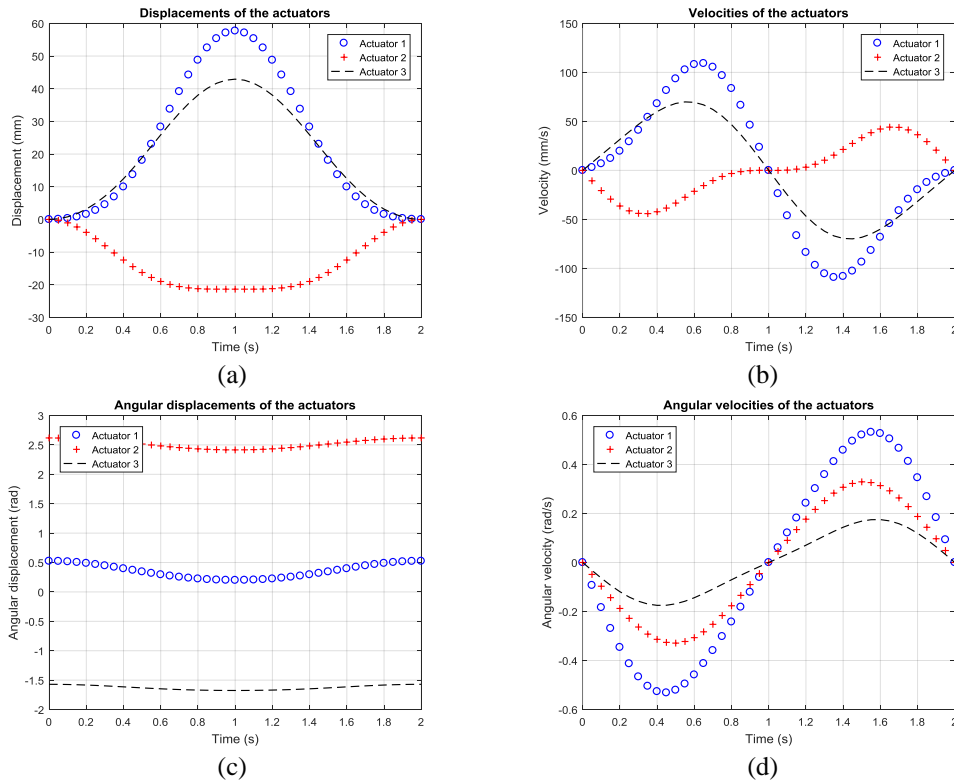


Figure 6 – Linear and angular displacements and velocities of the actuators.

Using the derivatives of the Jacobian matrices from the Eq. 7 and 11, the time response of the limbs was obtained for the input functions shown in Eq. 17. Figures 7.b and 7.d shows the linear and angular accelerations of the actuators and Fig. 7.a and 7.c shows the linear and angular velocities of the actuators, respectively, by integrating (with the corresponding boundary conditions) the accelerations of the actuators.

$$\begin{cases} \ddot{X} = 5.00\sin(\pi t) \text{ mm/s}^2 \\ \ddot{Y} = -5.00\sin(\pi t) \text{ mm/s}^2 \\ \ddot{\theta} = 0.0873 \text{ rad/s}^2 \end{cases} \quad (17)$$

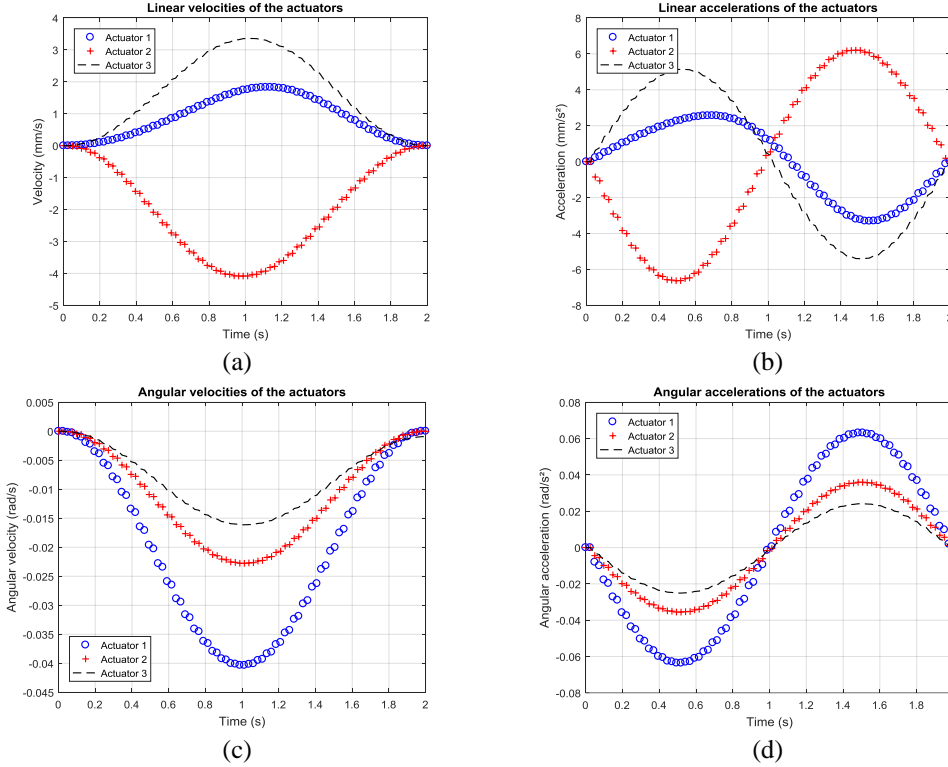


Figure 7 – Linear and angular velocities and accelerations of the actuators.

DYNAMIC MODEL USING POWER FLOW APPROACH

In this Section, will be presented the planar platform dynamics model from the kinematic model using power flow. At first, only one rigid body will be considered in the dynamic model of the manipulator: the mobile platform (with mass m_p and moment of inertia J_{pzz}). According to the described in Speranza Neto (2007), the Eq. 18 describes the Newton-Euler equations in that rigid body mobile local frame. The differential equations in the local frame are given in Eq. 19.

$$\begin{cases} \sum F_x = m_p(\dot{v}_X + v_Y\omega_Z) \\ \sum F_y = m_p(\dot{v}_Y - v_X\omega_Z) \\ \sum M_z = J_{pzz}\dot{\omega}_Z \end{cases} \quad (18)$$

$$\begin{cases} \dot{v}_X = \frac{\sum F_X}{m_p} - v_Y\omega_Z \\ \dot{v}_Y = \frac{\sum F_Y}{m_p} + v_X\omega_Z \\ \dot{\omega}_Z = \frac{\sum M_Z}{J_{pzz}} \end{cases} \quad (19)$$

According to Speranza Neto (1999), when possible, both completely match the power variables on the inputs and outputs of the subsystems (same type and direction of power flow) and a consistent cause and effect relation (which variables enter and which come out the models to be coupled), the resulting model is fully equivalent to that which would be obtained analytically, allowing your simulation from the simple connection of the modules. Considering this, the diagram (Fig. 8) that illustrates the relationships of cause and effect of the planar platform with three degrees of freedom is mounted.

With the kinematic relationships of this parallel mechanism comes the relation of consequence of the power conservation on the actuators coupling with the rigid body based on the inverse Jacobian (Eq. 2). Equations 20 to 22 presents the development of this relation. Using the same methodology, the relation of consequence of the power conservation on the actuators coupling with the rigid body based on \mathbf{J}_0^{-1} (Eq. 4) is shown in Eq. 23.

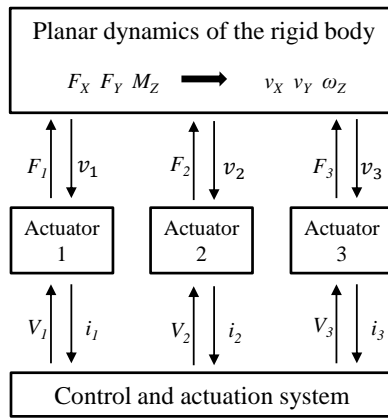


Figure 8 – Cause and effect relations of the planar platform.

$$P_{Rigid} = P_{Actuation} \Rightarrow [F_X \ F_Y \ M_Z]_{Body} \cdot \begin{bmatrix} v_X \\ v_Y \\ \omega_Z \end{bmatrix} = [F_1 \ F_2 \ F_3]_{System} \cdot \begin{bmatrix} v_1 \\ v_2 \\ v_3 \end{bmatrix} \quad (20)$$

$$[F_X \ F_Y \ M_Z] \cdot \begin{bmatrix} v_X \\ v_Y \\ \omega_Z \end{bmatrix} = [F_1 \ F_2 \ F_3] \cdot \mathbf{J}^{-1} \begin{bmatrix} v_X \\ v_Y \\ \omega_Z \end{bmatrix} \quad (21)$$

$$[F_X \ F_Y \ M_Z] = [F_1 \ F_2 \ F_3] \cdot \mathbf{J}^{-1} \Rightarrow \begin{bmatrix} F_X \\ F_Y \\ M_Z \end{bmatrix} = (\mathbf{J}^{-1})^T \begin{bmatrix} F_1 \\ F_2 \\ F_3 \end{bmatrix} \quad (22)$$

$$[F_X \ F_Y \ M_Z] = [M_1 \ M_2 \ M_3] \cdot \mathbf{J}_0^{-1} \Rightarrow \begin{bmatrix} F_X \\ F_Y \\ M_Z \end{bmatrix} = (\mathbf{J}_0^{-1})^T \begin{bmatrix} M_1 \\ M_2 \\ M_3 \end{bmatrix} \quad (23)$$

Considering the inertia effects of the moving platform, with mass m_p and mass moment of inertia J_{pzz} , the bond graphs structure of the direct dynamics model of the planar platform with three degrees of freedom is shown in Fig. 9. Using the concepts, elements and the graphical representation of the Bond Graph Technique, was further added the inertial effects of the bodies that compound the actuators, introducing the terms m_{Ai} and J_{Ai} , which correspond to the mass and moments of inertia of the actuators, with $i = 1, 2$ and 3 . It was also included in this model the equivalent viscous friction in the rotation joints. Figure 10 shows the same model using multibond graphs.

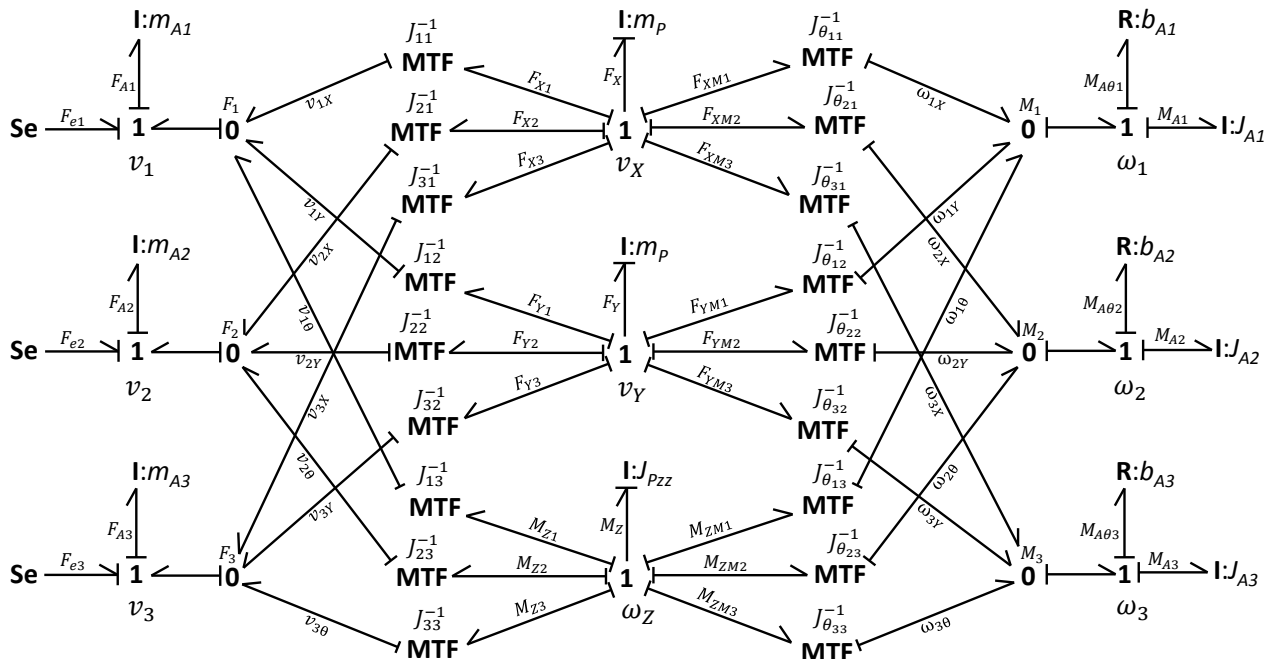


Figure 9 – Bond graphs representation of the planar platform dynamics.

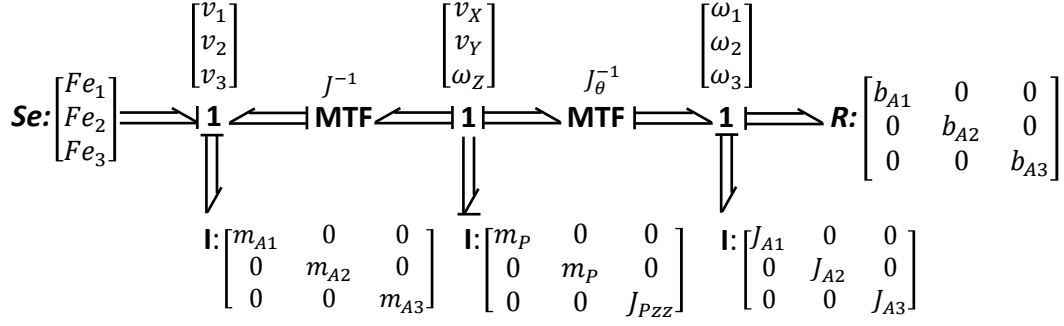


Figure 10 – Multibond graphs representation of the planar platform dynamics.

From the model in the Fig. 10, the constitutive equations of the inertia elements (I) with integral (or natural) causality are written in their differential form. Thus, making explicit the efforts, inserting this equation into the junction structures equations and replacing the constitutive equations of the inertial elements with differential (forced) causality, the resistors elements (R) and the modulated transformers (MTF), the Eq. 24 is obtained, where M_P , f_e , M_A , J_A and B_A are defined in Eq. 25 to 29, respectively.

$$\mathbf{M}_P \dot{v} = \mathbf{J}^T f_e - \mathbf{J}^T \mathbf{M}_A \dot{v}_A - \mathbf{J}_\theta^T \mathbf{J}_A \dot{\omega}_A - \mathbf{J}_\theta^T \mathbf{B}_A \omega_A \quad (24)$$

$$\mathbf{M}_P = \begin{bmatrix} m_P & 0 & 0 \\ 0 & m_P & 0 \\ 0 & 0 & J_{Pzz} \end{bmatrix} \quad (25)$$

$$f_e = \begin{bmatrix} F_{e1} \\ F_{e2} \\ F_{e3} \end{bmatrix} \quad (26)$$

$$\mathbf{M}_A = \begin{bmatrix} m_{A1} & 0 & 0 \\ 0 & m_{A2} & 0 \\ 0 & 0 & m_{A3} \end{bmatrix} \quad (27)$$

$$\mathbf{J}_A = \begin{bmatrix} J_{A1} & 0 & 0 \\ 0 & J_{A2} & 0 \\ 0 & 0 & J_{A3} \end{bmatrix} \quad (28)$$

$$\mathbf{B}_A = \begin{bmatrix} b_{A1} & 0 & 0 \\ 0 & b_{A2} & 0 \\ 0 & 0 & b_{A3} \end{bmatrix} \quad (29)$$

Substituting the equations from the derivatives of the Jacobian matrices (Eq. 7 and 11) and the Eq. 4 into the Eq. 24 and solving the algebraic loops associated to the storage elements with differential causality, the state-space equations are obtained (Eq. 30), with \mathbf{M}_1 and \mathbf{M}_2 given in Eq. 31 and 32, respectively.

$$\dot{v} = (\mathbf{M}_1^{-1} \mathbf{M}_2) v + (\mathbf{M}_1^{-1} \mathbf{J}^T) f_e \quad (30)$$

$$\mathbf{M}_1 = \mathbf{M}_P + \mathbf{J}^T \mathbf{M}_A \mathbf{J}^{-1} + \mathbf{J}_\theta^T \mathbf{J}_A \mathbf{J}_\theta^{-1} \quad (31)$$

$$\mathbf{M}_2 = -\mathbf{J}^T \mathbf{M}_A \dot{\mathbf{J}}^{-1} - \mathbf{J}_\theta^T \mathbf{J}_A \dot{\mathbf{J}}_\theta^{-1} - \mathbf{J}_\theta^T \mathbf{B}_A \mathbf{J}_\theta^{-1} \quad (32)$$

In the simulation of the dynamic model were considered the mass and the mass moment of inertia of the moving platform, m_P and J_{Pzz} , the mass and the mass moment of inertia of the actuators, m_{A1} , m_{A2} , m_{A3} and J_{A1} , J_{A2} , J_{A3} , and the viscous friction coefficients from the actuators joints, b_{A1} , b_{A2} and b_{A3} . Table 2 presents the parameters used in this simulation. The time response of the limbs was obtained for the inputs shown in Fig. 11. Two pulses with amplitudes 5 N and -5 N, widths of 0.1 s and interval of 0.1 s between them were given by the actuator 1. Figures 12.a and 12.b shows the linear and angular accelerations of the moving platform, Fig. 12.c and 12.d shows the linear and angular velocities of the moving platform and Fig. 12.e and 12.f shows the linear and angular displacements of the moving platform.

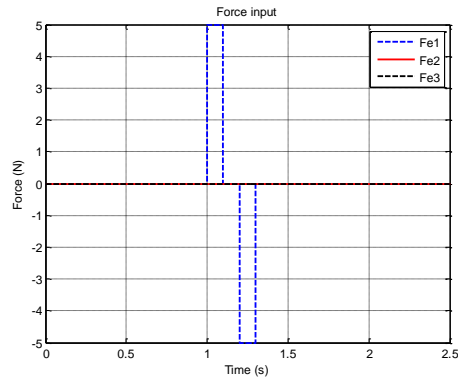
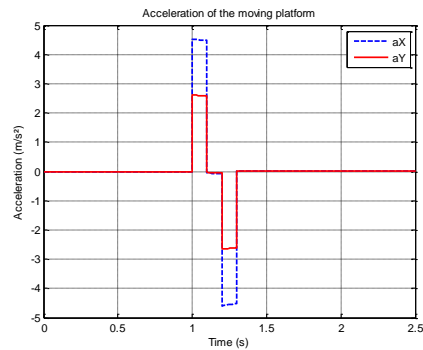


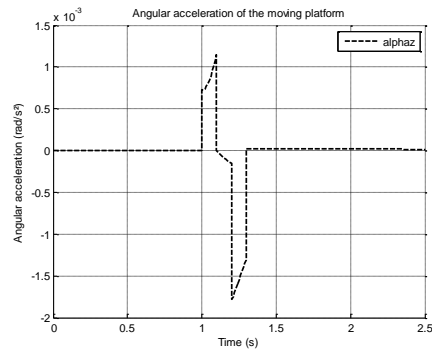
Figure 11 – Forces given by the actuators.

Table 2 – Planar mechanism simulation parameters.

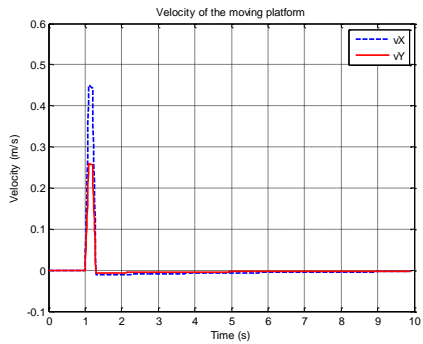
Identification	Symbol	Value
Mass of the platform (kg)	m_P	0.578
Mass moment of inertia of the platform ($\text{kg}\cdot\text{m}^2$)	J_{Pzz}	4.50×10^{-3}
Mass of the actuator rod (kg)	m_{A1}, m_{A2}, m_{A3}	0.175
Mass moment of inertia of the actuator ($\text{kg}\cdot\text{m}^2$)	J_{A1}, J_{A2}, J_{A3}	7.28×10^{-3}
Viscous friction coefficient of the joints ($\text{N}\cdot\text{s}\cdot\text{m}^{-1}$)	b_{A1}, b_{A2}, b_{A3}	0.006



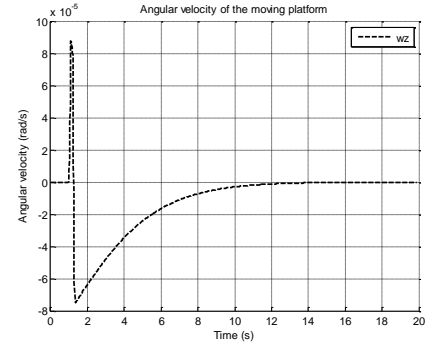
(a)



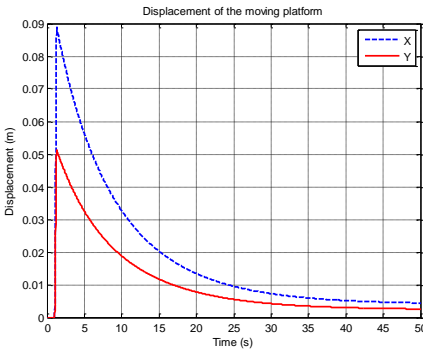
(b)



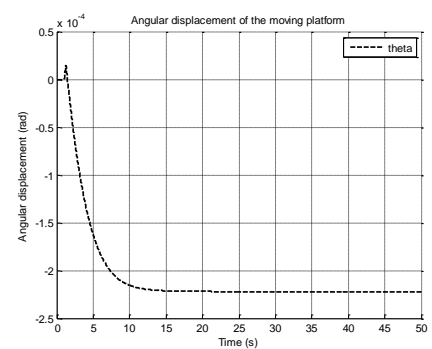
(c)



(d)



(e)



(f)

Figure 12 – Linear and angular accelerations, velocities and displacements of the moving platform.

CONCLUSIONS AND FUTURE WORK

In this work a procedure for the determination of the analytical form of dynamic models of a 3-RPR parallel mechanism through the characterization of the power flow between its components was presented. From the geometrical relations associated to the displacement of their degrees of freedom, the kinematic relations associated to their velocities were determined. Considering the power flow between the degrees of freedom and between these and the actuating elements, the equilibrium relations of the forces and torques were obtained. Also, inertial effects of system components, stiffness and damping effects were taken into account and the equations of motion were analytically determined. This approach adopted the same fundamentals, concepts and elements of the Bond Graph Technique.

A set of simulations were performed to validate this approach, using the real data (geometry, inertia, damping, actuators forces, etc) from a planar mechanism designed and built especially for the purpose to compare the simulated and experimental results. The ongoing work focuses in implement these models in the built platform in order to verify these responses on real environment.

ACKNOWLEDGMENTS

The authors of this work would like to thank FAPERJ and CNPq for the financial support.

REFERENCES

- Albuquerque, A.N., 2017, “Dinâmica e controle de mecanismos paralelos inseridos em uma estrutura HIL – hardware in the loop: integração modelo analítico fechado, transdutores inerciais e atuadores elétricos lineares”, In portuguese, Pontifical Catholic University, Department of Mechanical Engineering, Doctoral dissertation (unpublished), Rio de Janeiro, Brazil.
- Albuquerque, A.N., Speranza Neto, M. and Meggiolaro, M.A., 2016, “Dynamic models of parallel mechanisms using power flow approach”, CONEM 2016, IX Congresso Nacional de Engenharia Mecânica, Fortaleza, Brazil.
- Costa Neto, R.T., 2008, “Modelagem e integração dos mecanismos de suspensão e direção de veículos terrestres através do fluxo de potência”, In portuguese, Pontifical Catholic University, Department of Mechanical Engineering, Doctoral dissertation, Rio de Janeiro, Brazil.
- Karnopp, D.C., Margolis, D.L. and Rosenberg, R.C., 1990, “System dynamics: A unified approach”, 2nd Edition, John Wiley & Sons.
- Karnopp, D.C. and Rosenberg, R.C., 1968, “Analysis and simulation of multiport systems. The bond graph approach to physical system dynamics”, The M.I.T. Press.
- Martins, G.N., Speranza Neto, M. and Meggiolaro, M.A., 2016, “Dynamic models of bicycles and motorcycles using power flow approach”, CONEM 2016, IX Congresso Nacional de Engenharia Mecânica, Fortaleza, Brazil.
- Rosenberg, R.C. and Karnopp, D.C., 1983, “Introduction to physical system dynamics”, McGraw-Hill.
- Speranza Neto, M., 1999, “Procedimento para acoplamento de modelos dinâmicos através do fluxo de potência”, In portuguese, XV Brazilian Congress of Mechanical Engineering, São Paulo, Brazil.
- Speranza Neto, M., 2007, “Dinâmica de um corpo rígido através do fluxo de potência”, In portuguese, Pontifical Catholic University, Department of Mechanical Engineering, Lecture notes, Rio de Janeiro, Brazil.
- Speranza Neto, M. and Silva, F.R., 2005, “Modelagem e análise de sistemas dinâmicos”, In portuguese, Pontifical Catholic University, Department of Mechanical Engineering, Lecture notes, Rio de Janeiro, Brazil.
- Tsai, L.W., 1999, “Robot analysis – The mechanical of serial and parallel manipulators”, Department of Mechanical Engineering and Institute for Systems Research, University of Maryland, John Wiley and Sons, Inc., USA.
- Yildiz, I., Ömürlü, V.E. and Sagirli, A., 2008, “Dynamic modeling of a generalized Stewart platform by bond graph method utilizing a novel spatial visualization technique”, International Review of Mechanical Engineering, Turkey.
- Wang, Y., 2008, “Symbolic kinematics and dynamics analysis and control of a general Stewart parallel manipulator”, State University of New York at Buffalo, Department of Mechanical and Aerospace Engineering, Master’s thesis, Buffalo, USA.
- Zhao, Q. and Gao, F., 2012, “Bond graph modelling of hydraulic six-degree-of-freedom motion simulator”, Proceedings of the Institution of Mechanical Engineers, Part C: Journal of Mechanical Engineering Science, USA.

RESPONSIBILITY NOTICE

The authors are the only responsible for the material included in this paper.